Journal of Cerebral Blood Flow and Metabolism
13:733–747 © 1993 The International Society of Cerebral Blood Flow and Metabolism
Published by Raven Press, Ltd., New York

Measurement of Regional Cerebral Blood Flow with Positron Emission Tomography: A Comparison of [^{15}O]Water to [^{11}C]Butanol with Distributed-Parameter and Compartmental Models

Robert P. Quarles, *Mark A. Mintun, †‡Kenneth B. Larson, ‡Joanne Markham, §Ann Mary MacLeod, and †§Marcus E. Raichle

*Department of Radiology, University of Florida, Gainesville, Florida, *Division of Nuclear Medicine, University of Pittsburgh, Pittsburgh, Pennsylvania, and †Department of Neurology and Neurosurgery, ‡Institute for Biomedical Computing, and §Mallinckrodt Institute of Radiology, Washington University of Medicine, St. Louis, Missouri, U.S.A.*

Summary: To further our understanding of the best way to measure regional CBF with positron emission tomography (PET), we directly compared two candidate tracers ([^{15}O]water and [^{11}C]butanol, administered intravenously) and two popular implementations of the one-compartment (1C) model: the autoradiographic implementation representing a single PET measurement of tissue radioactivity over 1 min and a dynamic implementation representing a sequence of measurements of tissue radioactivity over 200 s. We also examined the feasibility of implementing a more realistic, and thus more complex, distributed-parameter (DP) model by assigning fixed values for all of its parameters other than CBF and tracer volume of distribution (V_d), a requirement imposed by the low temporal resolution and statistical quality of PET data. The studies were performed in three normal adult human subjects during paired rest and visual stimulation. In each subject seven regions of interest (ROIs) were selected, one of which was the primary visual cortex. The corresponding ROI were anatomically equivalent in the three subjects. Regional CBF, V_d, tracer arrival delay, and dispersion were estimated for the dynamic data curves. A total of 252 parameter sets were estimated. With [^{11}C]butanol both implementations of the 1C model provided similar results ($r = 0.97$). Flows estimated using the 1C models were lower ($p < 0.01$) with [^{15}O]water than with [^{11}C]butanol. In comparison with the 1C model, the constrained version of the DP used in these studies performed inadequately, overestimating high flow and underestimating low flow with both tracers, possibly as the result of the necessity of assigning fixed values for all of its parameters other than CBF and V_d. **Key Words:** Blood flow tracers—Brain activation—Compartmental models—Dispersion and delay—Distributed-parameter models—Positron emission tomography—Regional cerebral blood flow.

Various methods for measuring regional CBF (rCBF) with positron emission tomography (PET) have been proposed, both for functional brain mapping and for determination of cerebral metabolic supply–demand relationships. Many of these have employed [^{15}O]water as the tracer, primarily due to the short half-life of ^{15}O, which allows sequential studies and exposes the subject to a relatively low radiation dose. Although the methods of tracer administration vary, including continuous inhalation of [^{15}O]carbon dioxide (Frackowiak et al., 1980; Brooks et al., 1986; Lammertsma et al., 1989), single-breath inhalation of [^{15}O]carbon dioxide (Kanno et al., 1984), ramp intravenous infusion of [^{15}O]water (Ginsberg et al., 1982), and intravenous bolus injection of [^{15}O]water (Herscovitch et al., 1983; Huang et al., 1983; Raichle et al., 1983), most analyses of the resultant data are based on a one-

Received July 22, 1992; final revision received March 12, 1993; accepted March 15, 1993.

Address correspondence and reprint requests to Dr. M. E. Raichle at Division of Radiation Sciences, Mallinckrodt Institute of Radiology, Washington University School of Medicine, 510 S. Kingshighway, Campus Box 8225, St. Louis, MO 63110, U.S.A.

Abbreviations used: AR, autoradiographic; 1C, one-compartment; D1C, dynamic 1C; DP, distributed-parameter; PET, positron emission tomography; rCBF, regional CBF; ROI, region of interest.

compartment (1C) lumped-parameter model, originally applied to rCBF studies by Kety (1960).

One of the simplest implementations of the 1C model is the autoradiographic (AR) technique (Herscovitch et al., 1983; Raichle et al. 1983), in which only one parameter (rCBF) is estimated, using an independently measured tracer volume of distribution (V_d). It has been demonstrated that rCBF estimates by the AR method are sensitive to the length of PET data acquisition (Raichle et al., 1983; Ginsberg et al., 1984) and, to a much lesser degree, to variations in the local V_d (Herscovitch et al., 1983; Iida et al., 1986). Due in part to these difficulties, many recent efforts have focused on dynamic implementations of the 1C model that utilize longer data acquisition times and employ optimization to estimate both rCBF and the corresponding regional volume of distribution (Huang et al., 1982; Alpert et al., 1984; Koeppe et al., 1985; Carson et al., 1986). While these methods address known deficiencies of the AR technique, they share the basic assumption of the model on which they are based: that the tracer used is "freely diffusible," and thus that its clearance rate is flow limited. It has been well documented, however, that the diffusion of [^{15}O]water in the brain is not infinitely rapid (Eichling et al., 1974; Bolwig and Lassen, 1975; Raichle et al., 1976; Go et al., 1981; Herscovitch et al., 1987; Larson et al., 1987) and that this diffusion limitation may lead to underestimation of rCBF (Raichle et al., 1983; Kanno et al., 1984; Larson et al., 1987).

In the present study, we sought to determine what, if any, differences existed between the two most popular implementations of the 1C model and a two-barrier distributed-parameter (DP) model (Larson et al., 1987) that accounts for tracer diffusion limitations by carrying out paired PET studies using [^{15}O]water and [^{11}C]butanol as tracers. We analyzed our data on the basis of simulations employing the two above-mentioned tracer kinetic models: a 1C and a DP. The 1C model was applied under two different implementations: an autoradiographic (AR1C) and a dynamic (D1C). We estimated the parameter(s) of the D1C and the DP model by determining optimum fits of the individual model simulations to the data. Table 1 indicates the parameters that are estimated for each model implementation. As an integral part of these analyses, we have also accounted for the effects of delay and dispersion accompanying carriage of tracer in blood flowing in our sampling system and to any specified region of the brain. Both these effects have been shown to influence rCBF estimates from PET data (Koeppe et al., 1985, 1987; Carson et al., 1986; Iida et al., 1986; Kanno et al., 1987).

TABLE 1. *Summary of model parameters estimated*

Model	Tracer	Regional CBF	V_d	t_0	τ
Autoradiographic	[^{15}O]Water	E	0.90 ml/g	M	—
	[^{11}C]Butanol	E	0.77 ml/g	M	—
One-compartment dynamic	[^{15}O]Water	E	E	E	E
	[^{11}C]Butanol	E	E	E	E
Distributed-parameter dynamic	[^{15}O]Water	E	E	E	E
	[^{11}C]Butanol	E	E	E	E

V_d, volume of distribution parameter; t_0, differential delay parameter; τ, differential dispersion time constant; E, estimated from positron emission tomography data; M, measured from bank pair count rate records.

MATHEMATICAL MODELS

The 1C model

At present, most methods for measuring rCBF with [^{15}O]water and PET, including those used in our laboratory, are based on the 1C model originally proposed by Kety (1951, 1960). This model describes the behavior of a "freely diffusible" (i.e., flow-limited) tracer in a blood compartment and in a single tissue compartment, between which resistance to diffusive movement of tracer is vanishingly small. Thus, the kinetic behavior of this model is that of a single composite compartment. The derivation of the model equation is well known (Kety, 1951, 1960), and we shall not duplicate it here. The residue function unit impulse response of this model is $q^{\delta}(t) = \exp(-Ft/V_d)$, $t \geq 0$. Here, $q^{\delta}(t)$ is the quantity of tracer in a region at time t following administration of a unit bolus at $t = 0$, and F and V_d are the blood flow and the tracer volume of distribution in the region, respectively. If the input flux of tracer to the region is $Fc_a(t)$, where $c_a(t)$ is the tracer concentration history at the arterial inflow(s) to the region, then the residue function for the region is

$$q(t) = Fc_a(t) * q^{\delta}(t) = Fc_a(t) * \exp\left(\frac{-Ft}{V_d}\right) \qquad (1)$$

Here, the asterisks denote convolution.

The DP model

The DP model developed by Larson et al. (1987) for residue detection studies describes the transport of a chemically inert tracer that can pass bidirectionally between blood and tissue across a semipermeable membrane representing the blood–brain barrier. [A version of the present DP model suitable for outflow studies was developed by Rose et al. (1977).] In constructing the DP model, it is assumed that diffusive transport of tracer in tissue and in blood along the direction of blood flow is negligible relative to diffusive transport normal to that direction. It is also assumed that tracer transport lengthwise along a capillary occurs only at a finite speed

by carriage in flowing blood. In addition to the diffuse resistance offered by the blood–brain barrier, it is assumed that tracer diffusing radially in tissue encounters a finite distributed resistance there. Finally, it is assumed that the kinetic behavior of tracer in a macroscopic region of brain tissue is represented by the joint behavior in a large aggregation of independent capillary tissue units. These assumptions contrast sharply with the key assumption of the 1C model, that tracer encounters no diffusive transport resistance whatsoever in either blood or tissue, and with its corollary, that tracer transport is infinitely rapid in all directions. The solution of the tracer conservation equations of the DP model cannot be so compactly expressed as that of the 1C model, and we shall not quote the form of its unit impulse response here (see Larson et al., 1987). This model's incorporation of resistance to tracer diffusion has been shown, in comparison with the 1C model, to provide an improved description of the behavior of [^{15}O]water in the brain when used with data of temporal resolution higher than that achievable by PET (Larson et al., 1987).

Correction for dispersion and delay of tracer concentration histories in arterial blood

Our approach to correcting for the effects of dispersion and delay was motivated by the work of Iida et al. (1986, 1988, 1989) and of Kanno et al. (1987). These authors used the function $1 - e^{-t/\tau}$ to fit the experimental step response (normalized to the asymptotic steady state) of their catheter sampling system, finding that adequate fits over time (t) could be obtained by varying the single adjustable parameter (τ). Accordingly, we take as the unit impulse response of our sampling system the first time derivative of their unit step response, i.e., the function $(1/\tau)e^{-t/\tau}$. Following these authors, we have also incorporated in our approach a description of the effects of differential delay in the transport of tracer by flowing blood. Our resulting dispersion–delay correction function has the form

$$g(t;\tau,t_0,t_D) = u(t-t_0)\left(\frac{\bar{t}_D}{\tau}\right)\exp\left[-\frac{(t-t_0)}{\tau}\right],$$
$$\tau > 0,\ t_0 \geq 0,\ t_D > 0 \qquad (2;\ A16)$$

In it, the parameter τ accounts for differential dispersion effects, the parameter t_0 represents the time elapsed between the first appearance of tracer in a PET region of interest (ROI) and at the sampling detector, respectively, and the parameter $\bar{t}_D$ is the mean transit time of tracer through the sampling detector. In processing our data, we deconvolve our function $g(\cdot)$ with our automatic blood-sampling record, estimating both τ and t_0 along with the parameters of our physiological tracer transport models. The above-mentioned authors estimate only the delay parameter from their data, using values for "internal dispersion" premeasured in other subjects. Thus, our approach differs from that of these authors in that we estimate simultaneously the effects of dispersion and delay on a regional basis, from data for each subject, accounting for the effects arising during tracer transport to the sampling system detector and to each individual ROI in the brain. In Appendix we provide details concerning the derivation of the relations we use in implementing our method of correcting for dispersion and delay.

The methods of Lammertsma et al. (1989, 1990) and of Meyer (1989) are both similar to ours, but we have not utilized their equations because they are not applicable for use with our DP model. Further discussion of this point is given in Appendix.

METHODS

Paired [^{15}O]water and [^{11}C]butanol PET studies were performed in the resting state and during visual stimulation. The data obtained with each tracer were analyzed by using an autoradiographic (AR1C) and the dynamic implementation of the 1C model (D1C), as well as by using the DP model. The corresponding results for gray and white matter regions using all three approaches were compared.

PET studies in human subjects

PET studies were carried out for each of three normal male human subjects aged 26, 30, and 37 years. Informed consent was obtained from each subject prior to the studies, and all procedures were approved by the Human Studies Committee and the Radioactive Drug Research Committee of the Washington University School of Medicine. Each subject received two intravenous injections each of [^{11}C]butanol (35 mCi each injection) and [^{15}O]water (75 mCi each injection). The estimated dose equivalent for the complete study was 3.22 REMS, which is 64% of the allowable yearly dose of radioactivity for normal adult subjects as approved by the U.S. Food and Drug Administration [Federal Register 39 (no. 146) 27539-27540, 1974].

The PET studies were performed using the PETT VI tomograph (Ter-Pogossian et al., 1982), operating in the low-resolution mode with a resultant in-plane resolution of 11.7 mm full width at half-maximum and a slice thickness of 13.9 mm full width at half-maximum. Data were collected simultaneously for each of seven slices with a center-to-center separation of 14.4 mm between slices.

The subjects were placed on a tomography couch, and a 20-gauge catheter was placed in a radial artery under local anesthesia using 1% lidocaine. A second catheter was placed in the antecubital vein of the opposite arm for tracer injection. The subject's head was immobilized with a custom-fitted plastic mask fixed to the side of the couch

headrest. After positioning the subjects and couch in the tomograph, a lateral skull radiograph with radiopaque wires marking the center of each slice was obtained to document placement. A video monitor was then placed in front of the subjects, and it was verified that their field of view was unobstructed before draping the scanner and monitor to shield them from excess light. Transmission scans were obtained with a ^{68}Ge-^{68}Ga ring source to determine the attenuation characteristics of each subject's head. During all studies, background illumination was dimmed. The subjects' ears were unoccluded, and each subject could communicate easily with laboratory personnel throughout the study.

Each resting PET study was performed as follows. [^{15}O]Water was prepared by previously described methods (Welch et al., 1985). The subjects were instructed to close their eyes during this set-up period. One to two seconds prior to tracer injection, the subjects were instructed to open their eyes and to focus on a small white crosshair in the center of the video screen, the rest of which was blank. Coincident with intravenous bolus injection of ~75 mCi of [^{15}O]water, the PET scanner and arterial blood-sampling pump were started. Arterial blood sampling was accomplished by connecting the radial artery catheter through a three-way stopcock to a 0.050-in. inside-diameter plastic tube that ran through a plastic scintillator similar to that described by Hutchins et al. (1986). The length of tubing from the radial artery catheter to the exit of the scintillator was <45 cm. The scintillator response linearity had been previously verified up to 30,000 counts/s and was calibrated for each study against a standard well counter. Blood withdrawal was accomplished using a downstream peristaltic pump (Cole-Parmer 7525-34) operating at 0.4 ml/s from the time of injection (t = 0) to 90 s, at which time the flow rate was reduced to 0.05 ml/s. By 90 s, arterial tracer concentration was changing so slowly that the actual sampler flow had little influence on the sampler count rate. Total blood loss from each subject did not exceed 200 ml, and ~400 ml of normal saline was administered during each study. PET data acquisition consisted of 20 sequential 10-s scans separated by 1 s, beginning at 2 s after injection and continuing to 221 s. After ~10 min to allow for decay of ^{15}O (half-life = 122.1 s), the [^{15}O]water rest study was followed by a [^{11}C]butanol rest study. [^{11}C]Butanol was prepared as described by Herscovitch et al. (1987). An injection bolus of ~35 mCi was prepared, and the [^{11}C]butanol rest study was performed in a manner identical to the above-described [^{15}O]water study.

After ~60 min to allow for decay of ^{11}C (half-life = 20.28 min), a pair of PET studies was performed with visual stimulation. The paired visual stimulation study with [^{15}O]water and [^{11}C]butanol was performed exactly as described above, except that the crosshair on the video screen was surrounded by a red-and-black full-field annular checkerboard pattern with the colors reversing at a frequency of 10 Hz (Fox et al., 1987).

RCBF calculations

Dynamic images were reconstructed with an in-plane resolution of 18 mm. Sixty-second composite images were computed by summation of the counts in the first six 10-s frames. After global normalization, these composites were used to generate stimulus–rest subtraction images for both the [^{15}O]water and the [^{11}C]butanol pairs. The region of activation in the striate cortex was identified by simple visual inspection in each subtraction image, and a set of stereotaxic coordinates was established for that region (Fox et al., 1985). The resulting single set of coordinates was used to delineate the desired region for all calculations of primary visual cortex rCBF. For rCBF calculation, four frontal gray matter regions were chosen from among two contiguous slices of the composite images, as were two frontal white matter regions from the slice above. We ensured by stereotaxic means (Fox et al., 1985) that the selected regions were anatomically equivalent among the three subjects.

For estimating rCBF by the AR implementation of the 1C model, a single 43-s scan was formed by summing the counts for the first four 10-s frames, using linear interpolation between the frame midpoints to account for the counts lost during the 1-s data transfer intervals following each of the first three frames. For the D1C and the DP implementations, the entire data collection of 20 10-s frames was used. Parameter estimation for these methods was performed using a generalized nonlinear least-squares algorithm (Marquardt, 1963) to fit time-integrated model equations to the integrated PET scan data. Estimates of rCBF based on the AR technique were obtained using distribution volume values of $V_{d,w}$ = 0.90 ml/g for water (Herscovitch and Raichle, 1985) and $V_{d,b}$ = 0.77 ml/g for butanol (Gjedde et al., 1980). For the D1C implementation and the DP model, rCBF, distribution volume, differential delay time, and the differential dispersion time constant were estimated using all 20 frames of data for each of the two tracers (Table 1). The remaining parameters of the DP model were set to average values determined in previous studies employing it with [^{15}O]water as tracer (Larson et al., 1987). Among these were the capillary permeability–surface area product (PS), set at 130 ml min^{-1} hg^{-1}, and the tissue–blood partition coefficient (λ), set at 1.26. For processing the [^{11}C]butanol data with the DP model, the above values were retained, except for PS, set at 400 ml min^{-1} hg^{-1}, and for λ, set at 1.07. This value of PS corresponds to a tracer extracted fraction of 99.97% at a flow of 50 ml min^{-1} hg^{-1} (Larson et al., 1987).

Data analysis

First-order regression analysis was used to examine the relationships between estimates of flow obtained with butanol and water and the estimates obtained with butanol and the AR1C and the D1C method and the DP model.

Estimates of the y-intercept and the slope for the straight-line fits were computed by the method of unweighted least squares. Statistical significance tests were performed for the values of the y-intercept and the slope. The null hypotheses that the true intercept is 0 and that the true slope is 1 were tested by computation of the t test value for the estimated intercepts and slopes. For these analyses, all seven regional rCBF values were used for each PET study instead of the average values for gray and white matter as shown in Table 2.

The averaged rCBF values for white matter, gray matter, resting visual cortex, and stimulated visual cortex for each model–tracer combination were compared with the values obtained with the AR method and [^{11}C]butanol as the tracer using a paired t test. We chose this comparison because the AR method with [^{11}C]butanol has been directly compared with an independent standard and shown to yield a correct measurement of flow (Herscovitch et al., 1987).

TABLE 2. *Average rCBF estimates (ml min^{-1} hg^{-1})*

Tracer and model	White matter[a] (n = 12)	Gray matter[b] (n = 24)	Resting visual cortex[c] (n = 3)	Stimulated visual cortex[c] (n = 3)
[^{15}O]Water, AR	23.4 ± 3.6	46.2 ± 8.1[d]	41.7 ± 9.0	71.3 ± 9.6
[^{11}C]Butanol, AR	24.0 ± 2.8	51.3 ± 7.1	48.4 ± 15.7	81.3 ± 6.4
[^{15}O]Water, 1C dynamic	22.5 ± 2.6[d]	43.3 ± 6.0[d,e]	48.9 ± 8.6	63.8 ± 12.2
[^{11}C]Butanol, 1C dynamic	25.3 ± 4.3[d]	53.0 ± 8.3[d]	60.0 ± 16.0	89.9 ± 13.9
[^{15}O]Water, DP	21.2 ± 3.0	54.0 ± 12.3[d,e]	66.0 ± 23.0	115.3 ± 30.3
[^{11}C]Butanol, DP	20.2 ± 4.0	53.7 ± 11.7	64.9 ± 25.9[d]	135.9 ± 37.9

Values are ±SD. For abbreviations see the text.
[a] Averages over two regions, two states (resting and visual stimulation), and three subjects.
[b] Averages over four regions, two states (resting and visual stimulation), and three subjects.
[c] Averages over three subjects.
[d] Significantly different from [^{11}C]butanol with the AR method for same column using a paired t test at $p = 0.01$.
[e] Variances significantly different using an F test at $p = 0.01$; no other DP variance differs significantly from the corresponding AR or 1C dynamic variance at $p = 0.01$.

The averaged estimates of V_d obtained with the dynamic 1C and DP models for white matter, gray matter, and visual cortex are shown in Table 3. For each model–tracer combination, the average estimated V_d for white matter was compared with the average V_d for gray matter using a t test. In addition, for each model, the estimated values of V_d obtained for butanol for each region were compared with those obtained with water for the same region using a paired t test.

RESULTS

With [^{11}C]butanol as the tracer, the $D1C_b$ model shows an excellent correlation with the $AR1C_b$ (Fig. 1), but the $D1C_b$ slightly overestimates rCBF relative to the $AR1C_b$ (Fig. 1; Table 2).

Both implementations of the 1C model significantly underestimate CBF when using [^{15}O]water as the tracer (Fig. 2; Table 2) when compared with the $AR1C_b$ model. Although the responses we observe in resting and activated visual cortex are consistent with this result, our data are insufficient to independently establish the superiority of butanol over water in the measurement of functionally induced changes in blood flow. This must await a separate study directed specifically at this question and employing [^{11}C]butanol (Berridge et al., 1990, 1991).

In comparison with the $AR1C_b$, the DP model significantly overestimates rCBF at high flows and underestimates rCBF at low flows (Fig. 3), although it performs equally well with [^{15}O]water and [^{11}C]-butanol if data from activated visual cortex are excluded (Fig. 4).

The average effective regional V_d values calculated with the dynamic models are shown in Table 3. [As described in Methods, the value was fixed in the AR implementation of the 1C model at 0.90 ml/g (Herscovitch and Raichle, 1985).] For each method (model–tracer combination), the average estimated V_d for white matter regions was significantly less than the average V_d for gray matter regions ($p < 0.0001$), and for each model, estimates of V_d for butanol were significantly less than V_d for water in the same region ($p < 0.0001$) using a paired t test. Of particular note is the fact that the estimated V_d for the dynamic implementation of the 1C model (Table 3) is substantially lower than expected both for butanol (Gjedde et al., 1980) and water (Herscovitch and Raichle, 1985). This has also been noted by others (e.g., Lammertsma et al., 1990). Because a reduction in V_d usually leads to higher estimates of flow for the same tracer data set (Herscovitch and Raichle, 1983; Herscovitch et al., 1983; Larson et al., 1987), we wished to determine the effect of using the physiologically correct value of 0.90 ml/g for water (Herscovitch and Raichle, 1985) on the rCBF

TABLE 3. *Average distribution volume estimates (ml/g)*

Tracer and model	White matter[a]	Gray matter[a]	Resting visual cortex	Stimulated visual cortex
[^{15}O]water, 1C dynamic	0.579 ± 0.041	0.703 ± 0.078	0.650 ± 0.070	0.683 ± 0.064
[^{11}C]Butanol, 1C dynamic	0.433 ± 0.024	0.549 ± 0.048	0.565 ± 0.032	0.555 ± 0.040
[^{15}O]Water, DP	0.408 ± 0.031	0.562 ± 0.077	0.517 ± 0.056	0.516 ± 0.060
[^{11}C]Butanol, DP	0.310 ± 0.013	0.422 ± 0.040	0.433 ± 0.028	0.395 ± 0.033

Values are ±SD. For abbreviations see the text.
[a] For each method (model–tracer combination), the estimated V_d for white matter regions was significantly less than for gray matter regions ($p < 0.0001$). For each model, the estimated values of V_d obtained for butanol were significantly less than those for water ($p < 0.0001$) using a paired t test.

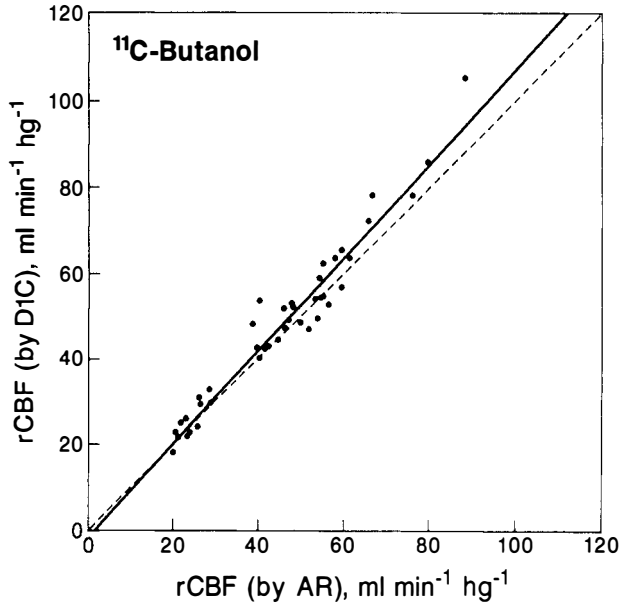

FIG. 1. The relationship between PET-measured rCBF in normal human subjects, using the same data set but analyzed with two implementations of the 1C model originally proposed by Kety (1957). The blood flow tracer was [^{11}C]butanol. On the *x*-axis are plotted data using the AR implementation of the 1C model (43 s of data collection) and on the *y*-axis data using the D1C model (220 s of data collection). The purpose of this comparison was to determine the accuracy of the D1C model in comparison with the previously empirically validated AR implementation (Herscovitch et al., 1987). The dashed line represents the line of identity. There is a significant correlation between the two methods of data analysis (r = 0.97). The solid line represents the linear regression line whose slope is slightly but significantly greater than 1 [1.09 ($p < 0.05$)] but whose intercept is not different from 0 [−1.45 (NS)]. For abbreviations see the text.

estimated with the dynamic implementation of the 1C model. To evaluate this, we compared the $AR1C_w$ and the $D1C_w$ methods using a fixed $V_{d,w}$ of 0.90 ml/g for both. Estimates of τ and t_0 obtained from the $D1C_w$ method (Tables 4 and 5) with four variable parameters were used for both methods; thus, for this comparison both the AR1C and the D1C methods estimated only one parameter, rCBF. Under these circumstances the dynamic implementation of the 1C model with 220 s of data collection significantly underestimated rCBF (Fig. 5), as expected.

Tables 4 and 5 list the average values for the differential delay (t_0) and the differential dispersion constant (τ). The latter was fixed at zero for the AR implementation. We would note for the interested reader that the apparent differences in Tables 4 and 5 are probably not significant. The optimization program we used did not compute the standard error of the estimated parameters. We suspect that the SEMs for t_0 and τ were very large and the correlation between them was high, implying that different values of the two parameters would yield approximately the same fitted curve. We would also note, as Meyer (1989) has done, that there is an inverse relationship between the delay and dispersion correction. This relationship implies that the variability associated with the estimates of both parameters is large and examination of only one of the parameter values does not give an accurate indication of the difference between individual cases.

DISCUSSION

The results of this study provide an opportunity to compare the three tracer kinetic strategies and two tracers for the measurement of rCBF with PET. In this study we have collected data from the cerebral cortex and underlying white matter of normal adult human subjects during rest and during physiological stimulation of the visual system. Each state has been studied with two different positron-emitting, radiolabeled tracers: water, the most widely used tracer for the measurement of rCBF with PET; and butanol, an attractive alternative because of its permeability characteristics (Raichle et al., 1976; Herscovitch et al., 1987; Berridge et al.,

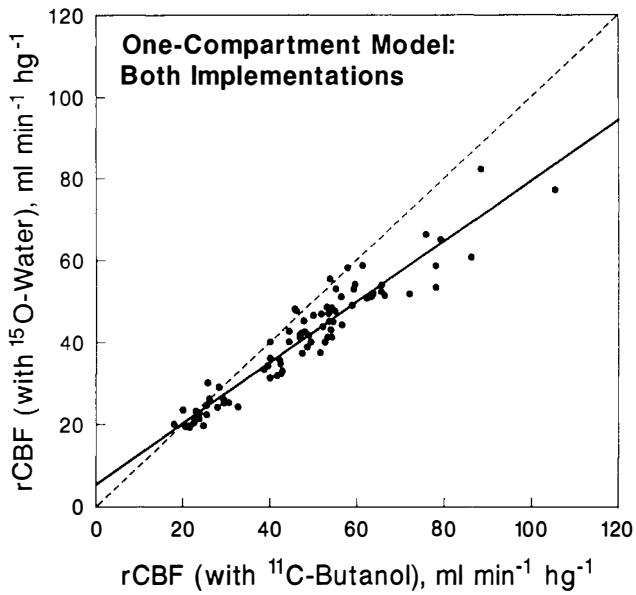

FIG. 2. A comparison of both implementations of the 1C model for the measurement of rCBF with PET using [^{11}C]-butanol (*x*-axis) and [^{15}O]water (*y*-axis). The purpose of this comparison was to determine whether the choice of tracer has a significant effect on the measured rCBF. The dashed line represents the line of identity. The solid line is the linear regression line. Although there is a significant correlation between the measurements made with these two tracers (r = 0.96), measurements made with [^{15}O]water significantly underestimate those made with [^{11}C]butanol [slope = 0.74 ($p < 0.01$); intercept = 5.6 ($p < 0.01$)], indicating that measurements made with butanol as the tracer more accurately reflect the true rCBF. For abbreviations see the text.

1990, 1991). We have analyzed these data with two implementations of the classic 1C model (Kety, 1951, 1960) and a constrained version of a more recently described DP model (Larson et al., 1987).

As a basis for comparison and discussion, we have chosen the autoradiographic implementation of the 1C model (Herscovitch et al., 1983; Raichle et al., 1983) using butanol as the tracer simply because this is the only PET strategy used for the measurement of rCBF with PET that has been directly compared with an independent standard and empirically found to be accurate over the range of flows examined in the present study (Herscovitch et al., 1987). In that validation study, Herscovitch et al. (1987) showed an excellent correlation between values obtained with the AR1C model and PET using [^{11}C]-butanol and those obtained with [^{15}O]water administered into the internal carotid artery in the same animal (i.e., rhesus monkey) and analyzed using residue detection and the central volume principle (Zierler, 1963).

Our results indicate that both implementations of the 1C model produce similar results. When employed with [^{11}C]butanol as the tracer, the D1C model exhibits an excellent correlation with the AR1C model, although a slight but significant tendency to overestimate rCBF is evident with the D1C method.

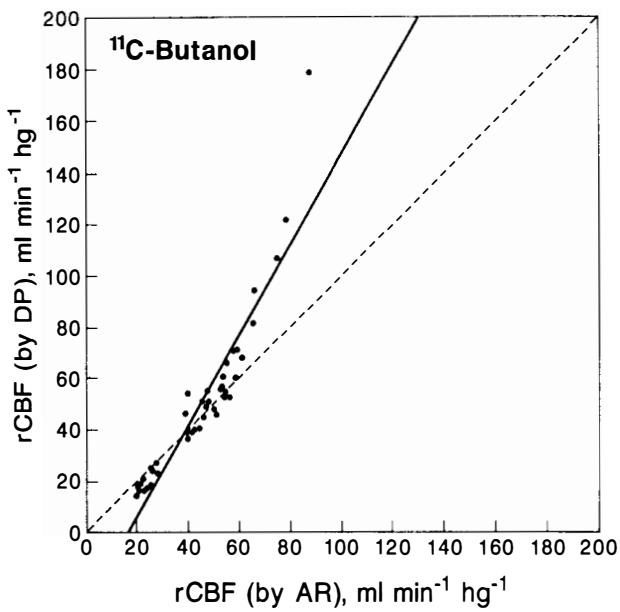

FIG. 3. The relationship between PET-measured rCBF in normal human subjects, using the same data set but analyzed with the AR implementation of the 1C model (*x*-axis) and the DP model (*y*-axis). The purpose of this comparison was to determine the accuracy of the DP model in comparison with the previously empirically validated AR implementation of the 1C (Herscovitch et al., 1987). The blood flow tracer was [^{11}C]butanol. The dashed line is the line of identity and the solid line is the linear regression line. Although there is a significant correlation between the two methods (r = 0.93), the DP significantly overestimates rCBF at flows >50 ml min^{-1} hg^{-1} and underestimates rCBF at flows less than ~30 ml min^{-1} hg^{-1}. For abbreviations see the text.

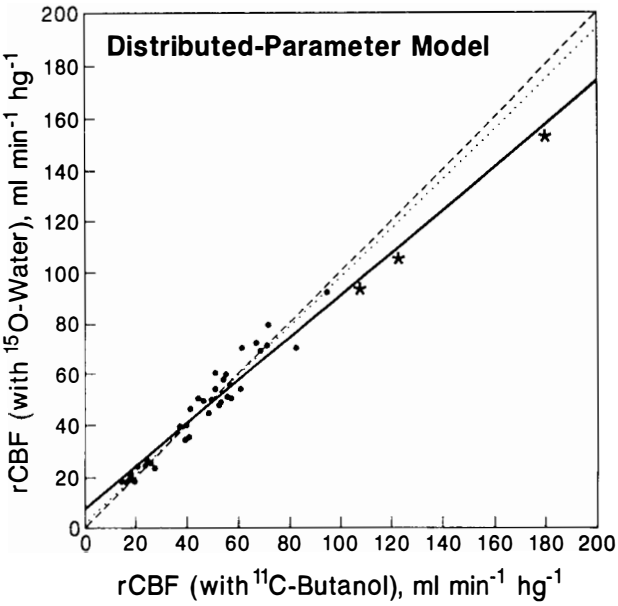

FIG. 4. A comparison of the performance of the DP model for the measurement of rCBF with PET using [^{11}C]butanol (*x*-axis) and [^{15}O]water (*y*-axis). The purpose of this comparison was to determine whether the choice of tracer influenced the results obtained with the DP model. The rCBF data obtained during the resting condition are shown as circles, whereas data obtained from stimulated visual cortex are shown as asterisks. The line of identity is the dashed line. The dotted line represents the linear regression line through the resting data [dots; slope = 0.96 (NS); intercept = 2.34 (NS)], whereas the solid line represents the regression line throughout all data points [dots + asterisks; slope = 0.84 ($p < 0.01$); intercept = 7.18 ($p < 0.01$)]. These data demonstrate that the DP model adequately accounts for the permeability differences between water and butanol in the resting brain but does significantly less well in physiologically activated cortex. Because the blood–brain barrier permeability was a fixed parameter in the DP model for these studies, this difference may reflect changes in the barrier permeability for water induced by physiological activation. For abbreviations see the text.

Both implementations of the 1C model underestimate CBF when employed with the tracer [^{15}O]water. This result is to be expected because the 1C model assumes that the tracer employed is freely permeable (Kety, 1951), but the permeability of the blood–brain barrier to water is known to be limited (Eichling et al., 1974; Herscovitch et al., 1987). As expected, the permeability limitation of [^{15}O]water is most evident at higher blood flows (Fig. 2). Because butanol transport is essentially flow limited at blood flows normally encountered in the human brain (Herscovitch et al., 1987), it is clearly a more desirable tracer for accurate measurements of CBF with PET in humans than

TABLE 4. *Average estimates of t_0 (s), differential delay paramter*

Tracer and model	White matter	Gray matter	Resting visual cortex	Stimulated visual cortex
[^{15}O]Water, 1C dynamic	7.4 ± 2.2	8.5 ± 2.2	6.2 ± 0.5	6.4 ± 1.0
[^{11}C]Butanol, 1C dynamic	8.2 ± 2.2	10.2 ± 2.5	8.0 ± 0.3	7.1 ± 1.5
[^{15}O]Water, DP	7.3 ± 2.0	10.2 ± 2.5	6.8 ± 1.6	8.0 ± 1.2
[^{11}C]Butanol, DP	7.1 ± 2.4	10.1 ± 1.5	7.2 ± 0.5	6.5 ± 1.8

Values are ±SD. For abbreviations see the text.

[^{15}O]water whenever implementations of the 1C model are used to process the data.

An alternative, although unlikely, explanation for the higher estimates of flow with [^{11}C]butanol would be the increased uptake of labeled metabolites of butanol by the brain, especially in high flow areas. Although we did not check the blood for the presence of metabolites of [^{11}C]butanol, we do not think the accumulation of metabolites in brain could account for the difference observed between [^{11}C]-butanol and [^{15}O]water for the following reasons. First, the well-documented difference in brain permeability of the two tracers is sufficient to account for the observed difference. Second, the difference in measured blood flow does not appear to be a systematic function of time after tracer administration, as might be expected if metabolite accumulation is occurring in the brain (see Table 2). Third, when differences in tracer permeability are explicitly accounted for, as in the DP model, no differences are observed in resting blood flow. Finally, empirical validation of the AR1C model with [^{11}C]-butanol (Herscovitch et al., 1987) showed an excellent correlation between values obtained with the AR1C model using [^{11}C]butanol and those obtained with [^{15}O]water administered into the internal carotid artery in the same animal (i.e., rhesus monkey) and analyzed using residue detection and the central volume principle. Such a result would be inconsistent with the accumulation of significant metabolites in brain tissue during the period of measurement.

Our results argue for the use of butanol as the tracer of choice with the 1C model. However, [^{11}C]butanol has two significant disadvantages when compared with [^{15}O]water: It is more difficult to synthesize (Herscovitch et al., 1987), and ^{11}C has a much longer half-life than ^{15}O (i.e., 20 min vs. 122 s). The longer half-life of ^{11}C is especially burdensome if multiple measurements are to be made in a single experiment (e.g., Petersen et al., 1988). As a result of the longer half-life, significantly more time must elapse between measurements to allow for the decay of the administered isotope (e.g., assuming 5 half-lives to be a satisfactory interval, this would be ~100 min for [^{11}C]butanol compared with 10 min for [^{15}O]water). Also, the longer half-life of ^{11}C means that less activity can be administered due to the higher radiation dose. Fortunately, a synthesis for [^{15}O]butanol has recently been developed (Berridge et al., 1990, 1991), which provides us with a tracer that combines an ideal half-life with satisfactory blood–brain barrier permeability characteristics and a relatively straightforward synthesis.

As an extension of the above discussion, it would be tempting to conclude that butanol is superior to water as a tracer for the special circumstance of functional brain-mapping studies with PET (e.g., see Petersen et al., 1988; Wise et al., 1991; Zatorre et al., 1992). Our data are insufficient to support that claim. Inspection of the data in Table 2 (resting and stimulated visual cortex) for both implementations of the 1C model reveals considerable variability even though results from [^{11}C]butanol are always higher than those from [^{15}O]water. We postulate that this variability is the result of three factors. First, in contrast to the remainder of our data set, information on visual cortex was limited to three observations. Second, for [^{11}C]butanol we injected half as much activity because of the radiation dose limits (35 vs. 75 mCi for [^{15}O]water). One should appreciate that the noise for the [^{11}C]butanol data

TABLE 5. *Average estimates of τ (s), differential dispersion parameter*

Tracer and model	White matter	Gray matter	Resting visual cortex	Stimulated visual cortex
[^{15}O]WaterWater, 1C dynamic	4.6 ± 2.3	4.3 ± 1.5	2.9 ± 2.5	7.0 ± 1.8
[^{11}C]Butanol, 1C dynamic	2.1 ± 2.8	1.1 ± 1.5	0.082 ± 0.14	2.6 ± 2.1
[^{15}O]Water, DP	5.2 ± 2.3	0.65 ± 1.2	0.055 ± 0.096	0.58 ± 1.0
[^{11}C]Butanol, DP	6.2 ± 4.4	0.17 ± 0.63	<0.01	<0.01

Values are ±SD. For abbreviations see the text.

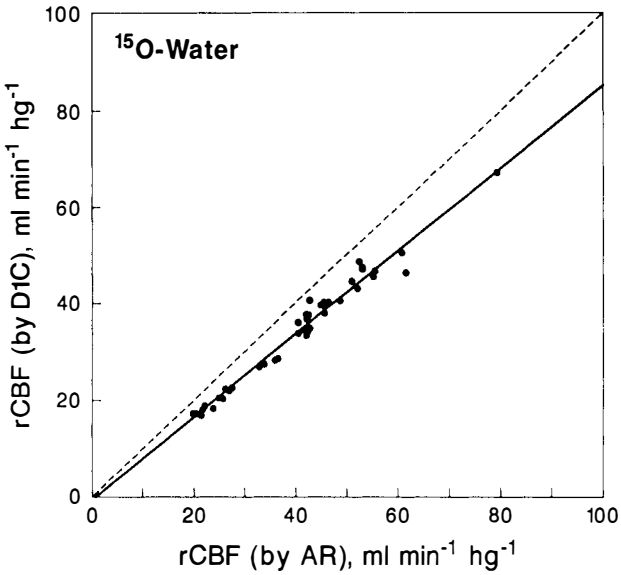

FIG. 5. A comparison of the AR implementation of the 1C model (*x*-axis) with the D1C model (*y*-axis) for the measurement of rCBF with PET. A fixed $V_{d,w}$ of 0.90 ml/g was used for both implementations. Differential dispersion (τ) and delay (t_0) were estimated using the D1C model with four variables and applied to both implementations. The purpose of this comparison was to determine whether a tendency to underestimate rCBF would be unmasked in the D1C model, with its data collection time of 220 s, when a physiologically reasonable $V_{d,w}$ was employed. The solid line is the linear regression line. The dashed line represents the line of identity. In this comparison, the D1C implementation significantly underestimates rCBF as compared with the AR implementation [slope = 0.86 ($p < 0.01$); intercept = −0.73 (NS)], supporting the hypothesis that the potential for a time-dependent underestimation of rCBF exists with this implementation of the 1C model. For abbreviations see the text.

will be proportionately increased. Finally, our data suggest that the permeability–surface area product for water may actually increase during physiological activation (see further discussion below). If that is, indeed, the case, then water may actually gain some advantage in relation to butanol under the special circumstances of functional activation studies. These issues remain to be clarified by further experiments employing [^{15}O]butanol to look at the special case of brain functional activation.

Our observations that the V_d estimated by the dynamic implementation of the 1C model is substantially lower than expected for both butanol (Gjedde et al., 1980) and water (Herscovitch and Raichle, 1985) despite a correct estimate of flow confirm work by previous investigators (e.g., see Lammertsma et al., 1990). One might wonder why the dynamic implementation of the 1C model seems systematically to underestimate the V_d and yet provide an accurate estimate of the blood flow. Why not a misestimation of both parameters of the model? Why not flow instead of V_d? The answer can be found in a consideration of the model Eq. 1, where it can be seen that flow (F) appears in two places, in the input function as well as the exponential unit impulse clearance function. The V_d appears only in the exponential clearance factor. The tracer washout rate predicted by the impulse response (i.e., bolus injection response) of the 1C model is slower than that actually observed (Larson et al., 1987, Fig. 4). This behavior is offset, and in effect corrected for, by the presence of F in the input function, causing the estimate of flow from early data to be more nearly correct. Indeed, the presence of F in the input function practically ensures correct estimation of flow with almost any model of tracer clearance when used before substantial clearance has occurred: This, of course, is the basis for the microsphere methods, in which there is no tracer clearance at all. As a result, F is more sensitively estimated, especially during tracer accumulation in the tissue (i.e., early in data collection). The estimation of V_d must await clearance of tracer from the tissue. As a result the flow is correctly estimated before the V_d and the latter parameter become dependent upon the estimate of flow (i.e., the two parameters are not estimated independently). This explanation is entirely consistent with our earlier observation that the AR implementation of the 1C model is insensitive to the choice of the V_d (Herscovitch et al., 1983, Fig. 1), and the dynamic implementation of the 1C model is quite sensitive (Fig. 4, this work). These relationships can also be more formally appreciated by computing the sensitivity functions (Beck and Arnold, 1977) for F and V_d of the 1C model.

Our data have two practical implications for the measurement of rCBF with PET. First, one should not employ the AR implementation of the 1C model, with its fixed V_d, beyond 1 min of data collection because increasing underestimation of CBF occurs with increasing data collection time, an effect that has been noted for the 1C model previously (Eklöf et al., 1975; Gambhir et al., 1987; Larson et al., 1987). Second, if it is deemed advantageous to extend data collection for a longer period of time, the use of the dynamic implementation of the 1C model is a wise choice, allowing estimates of both the flow and the V_d. Although V_d will then be systematically underestimated, a satisfactory estimate of CBF will be obtained, as we have shown in this study.

One of the objectives of this research was to evaluate a PET implementation of a two-barrier, DP model of water transport in brain developed in our laboratory for the measurement of rCBF (Larson et al., 1987). The development of this model was mo-

tivated by the inadequacy of the 1C model to describe the transport of labeled water in brain tissue (Ecklöff et al., 1974; Larson et al., 1987). Initial studies of the DP model with data of low spatial but high temporal resolution [i.e., externally detected residue curves following the intracarotid injection of [^{15}O]water in monkeys (Larson et al., 1987)] indicated that this model was superior to the 1C model as well as to a two-compartment and to a one-barrier DP model. However, PET data of the type used in the present study do not approach the temporal resolution or statistical quality of the data used in that original study. As a result it was necessary to constrain all of the parameters of the model except the flow and the V_d. This may explain the fact that estimates of flow using the DP model were appreciably lower than our standard (i.e., $AR1C_b$) at low flows and appreciably higher at high flows (Fig. 4). Additionally, estimates of V_d for both water and butanol were lower than expected (Herscovitch et al., 1987), a finding similar to that obtained with the dynamic implementation of the 1C model (Table 3). In the case of the DP model, we hypothesize that the low V_d estimates result from adverse effects of constraining the other parameters that were not estimated. We await future improvements in the temporal resolution of PET devices for deciding this issue.

It is of interest to note that our implementation of the DP model (Larson et al., 1987) obtains identical results with [^{15}O]water and [^{11}C]butanol in resting cerebral cortex and underlying white matter (Fig. 4). This is to be expected because the model explicitly accounts for the permeability of the blood–brain barrier (Larson et al., 1987). However, results from activated visual cortex (Fig. 4) indicate that with this model, [^{15}O]water provides a lower estimate for rCBF than [^{11}C]butanol. We hypothesize that this discrepancy could be due to changes in the blood–brain barrier PS for water (PS_w) during neuronally induced increases in rCBF. Because our data sets are insufficient to estimate all of the parameters of the DP model including PS_w, a fixed value of 130 ml min^{-1} hg^{-1} was chosen [a previous estimate of PS_w in resting human visual cortex was 127 ml min^{-1} hg^{-1} (Herscovitch et al., 1987)]. The same value was applied to both resting and activated visual cortex. Using the approach of Herscovitch et al. (1987), we can estimate from the data in Table 2 of the present experiments that stimulated visual cortex PS_w may have risen to 169 ml min^{-1} hg^{-1} from 100 ml min^{-1} hg^{-1}. We could have used such specific estimates of PS_w for white and gray matter and visual cortex rather than a fixed value. This could have been accomplished by using the strategy of Herscovitch et al. (1987) and the present data analyzed with $AR1C_w$ and $AR1C_b$. However, this would have defeated our present objective of evaluating the DP model as a "stand-alone" means of estimating rCBF with PET.

In conclusion, both implementations of the classic 1C model tested in this study give comparable results when used to measure rCBF with PET. The use of butanol as a tracer, rather than water, avoids the underestimation of flow by both implementations of the 1C model due to the permeability limitation of water in brain, which is not accounted for in that model. Time-dependent underestimation of rCBF is a potential problem with either implementation of the 1C model. It is avoided in the AR1C implementation by restricting data collection to <1 min, and in the D1C implementation by accepting V_d estimates less than the known physiological values. Finally, although we have shown our DP model to realistically describe tracer movement in brain (Larson et al., 1987), the inherent limitation of PET data itself (i.e., temporal resolution and statistical quality) precludes the satisfactory implementation of our DP model for the routine measurement of rCBF with current PET machines. The DP model remains for us, however, a very useful conceptual tool for the understanding of the behavior of inert tracers in the brain in the same spirit that theoretical models have become increasingly useful in conceptualizing our understanding of other areas of neuroscience.

APPENDIX

Dispersion and Delay Modeling

We provide here derivations of the relations used to account for the effects of temporal dispersion and delay in blood concentration histories that arise during carriage of tracer by blood in arteries and arterioles and through our automatic blood-sampling system.

Figure 6 shows two paths followed by flowing arterial blood while carrying tracer after its intravenous injection. In Branch I, some of the tracer arriving at the arch of the aorta is carried from there through arteries and arterioles to a selected ROI in brain. Meanwhile, in Branch II, another portion of the injected tracer is carried from the aortic arch to a peripheral artery blood-sampling site and from there, via a sampling catheter, through the sensitive volume of the sampling system scintillation detector. At the inlet to each of the two branches, the concentration of tracer is described by a *common* history, $[c(t)]$, but as tracer is carried through each branch, the initial history becomes dispersed.

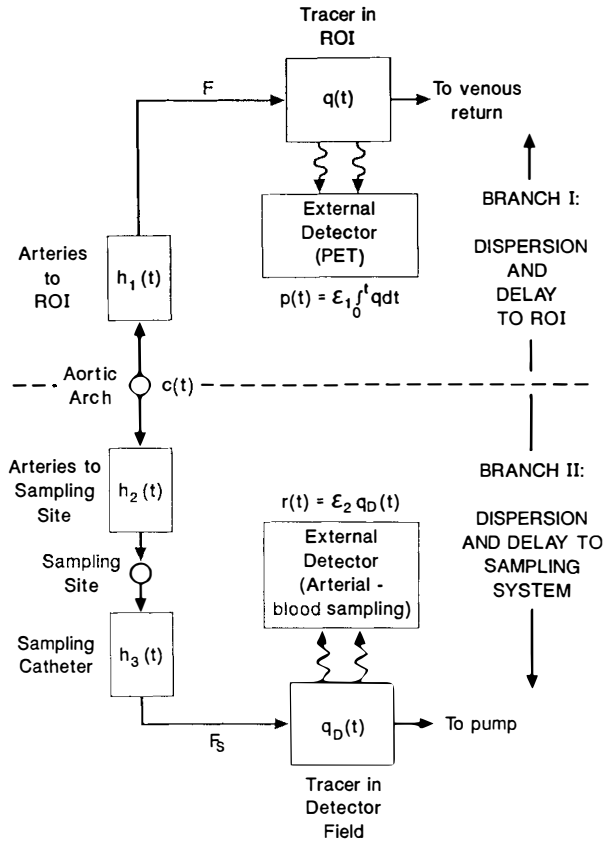

FIG. 6. Schematic diagram of paths followed by flowing arterial blood while carrying tracer leaving the heart. Branch I: path via arteries to a region of interest (ROI). Branch II: path via arteries to peripheral blood-sampling site, sampling catheter, and scintillation detector. Blood flow value in ROI is denoted F; through the detector, F_s. At the inlet to each of the two branches, the time-varying concentration of tracer in blood common to the two branches is denoted $c(t)$. The outflow functions $h_1(t)$, $h_2(t)$, and $h_3(t)$ describe dispersion and delay of tracer flux in each branch. The time-varying amount of tracer in the ROI is denoted $q(t)$; the analogous tracer quantity in the detector field, $q_D(t)$. Radioactive decay of these tracer amounts gives rise to externally detected dynamic responses $p(t)$ and $r(t)$, respectively. These responses are processed by algorithms based on models of tracer transport (see text) to yield estimates of blood flow and tracer distribution volume in the ROI and of tracer dispersion and delay in the two flow branches.

Moreover, because of the finite speed of the flowing blood, the concentration history becomes delayed in time. In general, the degree of dispersion and delay in the two branches will not be the same, and in our approach we model the differential influence on the responses of the PET device and of the automatic blood-sampling system.

The observed PET response $[p(t)]$ to the time-varying quantity of tracer in the ROI $[q(t)]$ is expressed by

$$p(t) = \epsilon_1 \int_0^t q(\theta)d\theta \qquad \text{(A1)}$$

Here and in the following, $t = 0$ corresponds to the first appearance of tracer in the aortic arch, and ϵ_1 is a detection efficiency determined in calibration measurements using a phantom that incorporates known quantities of tracer. To infer brain blood flow and the tracer distribution volume from the PET measurements by parameter estimation, we compute a simulated PET response $[\hat{p}(t; \boldsymbol{x})]$ according to

$$\hat{p}(t; \boldsymbol{x}) = \epsilon_1 \int_0^t \hat{q}(\theta; \boldsymbol{x})d\theta \qquad \text{(A2)}$$

In the above, ϵ_1 is the same as in Eq. A1, and $\hat{q}(t; \boldsymbol{x})$is a simulation, on the basis of one of our tracer kinetic models, of the tracer content history of an ROI. Each of our tracer kinetic models incorporates a set $[\boldsymbol{x} = \{x_1, x_2, \cdots\}]$ of physiological parameters x_i; these can be, for example, blood flow, distribution volumes, compartmental rate constants, or others. The simulated tracer content of the ROI is given by

$$\hat{q}(t; \boldsymbol{x}) = Fc(t) * h_1(t) * q^{\delta}(t; \boldsymbol{x}) \qquad \text{(A3)}$$

[The * means convolution; for example, $c(t) * h_1(t) \triangleq \int_0^t c(\theta)h_1(t - \theta)d\theta$. Here and below, θ is a dummy variable of integration.] In Eq. A3, $q^{\delta}(t; \boldsymbol{x})$ is the *residue* function unit impulse response for any specified tracer kinetic model, F is the blood flow to the ROI (itself one of the parameters in $\boldsymbol{x}$), and $h_1(t)$ is the *outflow* function unit impulse response describing dispersion and delay in the arterial path from the aorta to the ROI. Thus, $h_1(t)$ represents dispersion and delay from the aorta *all the way to the PET ROI,* not just to, say, the common carotid artery. On combining Eqs. A2 and A3, we have

$$\hat{p}(t; \boldsymbol{x}) = \epsilon_1 F \int_0^t c(\theta) * h_1(\theta) * q^{\delta}(\theta; \boldsymbol{x})d\theta \qquad \text{(A4)}$$

for our simulation of the dispersed and delayed PET response in terms of any one of our chosen model unit impulse responses, $q^{\delta}(t; \boldsymbol{x})$.

The sampling system counting rate history $[r(t)]$ is related to the time-varying quantity of tracer $[q_D(t)]$ in its detector field of view (D) according to

$$r(t) = \epsilon_2 q_D(t) \qquad \text{(A5)}$$

Here, ϵ_2 is a detection efficiency defined by

$$\epsilon_2 \triangleq \frac{r_\infty}{V_D c_0}, \qquad \text{(A6)}$$

where V_D is the volume of sampled blood contained in D and r_∞ is the steady-state counting rate registered by the detector in response to a step input of

concentration $[c_0u(t)]$ that we impose during a separate calibration measurement. [Here, $u(t)$ is the unit step function.] In the calibration measurement, the quantity we determine is not ϵ_2 directly, but rather $r_\infty/c_0 = V_D\epsilon_2$; the significance of this becomes apparent below in passage from Eq. A17 to A18. The history of the quantity of tracer in $D[q_D(t)]$ is given by

$$q_D(t) = F_S c(t) * h_2(t) * h_3(t) * q_D^\delta(t) \quad \text{(A7)}$$

In the above, F_S is the volumetric rate at which sampled arterial blood is drawn through the sampling system, $h_2(t)$ is the *outflow* function dispersion delay unit impulse response for the arterial path from the aortic arch to the peripheral artery sampling site, $h_3(t)$ is the analogous response of the sampling system catheter from the sampling site to the inflow of D, and $q_D^\delta(t)$ is the *residue* function unit impulse response for tracer in D. On combining Eqs. A5 and A7, we obtain

$$\begin{aligned} r(t) &= \epsilon_2 F_S c(t) * h_2(t) * h_3(t) * q_D^\delta(t) \\ &= \epsilon_2 F_S c(t) * h_2(t) * q_S^\delta(t) \end{aligned} \quad \text{(A8)}$$

for the counting rate of the sampling system detector. In the above, we have defined the sampling system unit impulse response as $q_S^\delta(t) \triangleq h_3(t) * q_D^\delta(t)$. Eliminating $c(t)$ between Eqs. A4 and A8, we find for our simulated PET response:

$$\hat{p}(t; \mathbf{x}) = \frac{\epsilon_1 F}{\epsilon_2 F_S} \int_0^t [g(\theta)]^{-1} * r(\theta) * q^\delta(\theta; \mathbf{x}) d\theta \quad \text{(A9)}$$

Here, we define a function $g(t)$ such that the relation

$$g(t) * h_1(t) = h_2(t) * q_S^\delta(t) \quad \text{(A10)}$$

holds. {The notation $[g(t)]^{-1} * [\cdot]$ denotes deconvolution, the inverse of the operation of convolution.}

If dispersion and delay were the same in the sampled branch as in the ROI branch, then the relations $h_1(t) = h_2(t)$ and $g(t) = q_S^\delta(t)$ would hold, and no corrections for dispersion and delay would be necessary. In this case, the PET simulation would be merely

$$\hat{p}(t; \mathbf{x}) = \frac{\epsilon_1 F}{\epsilon_2 F_S} \int_0^t [q_S^\delta(\theta)]^{-1} * r(\theta) * q^\delta(\theta; \mathbf{x}) d\theta$$

In general, however, the effects are different in the two branches and the differences must be accounted for. Rather than model the effects in the two branches separately, we assume instead that the following empirical parameterized form for the function $g(t)$,

$$g(t; \tau, t_0, \Theta) = u(t - t_0) \frac{\Theta}{\tau} \exp\left(-\frac{t - t_0}{\tau}\right)$$
$$\tau > 0,\ t_0 \geq 0,\ \Theta > 0 \quad \text{(A11)}$$

can model not only the sampling system unit impulse response $[q_S^\delta(t)]$, but the *differential* dispersion and delay as well: The parameter τ accounts for the *difference* in the effects of dispersion in the two branches of Fig. 6 and the differential delay parameter t_0 represents the time elapsed *between* the first appearance of tracer in an ROI and in D, respectively. Here, Θ is a constant having dimensions of time that we evaluate as follows: Combining the Laplace transforms of A10 and A11, we obtain

$$\begin{aligned} G(s; \tau, t_0, \Theta) &= \left[\frac{H_2(s)}{H_1(s)}\right] Q_S^\delta(s) = \left[\frac{H_2(s)}{H_1(s)}\right] H_3(s) Q_D^\delta(s) \\ &= e^{-t_0 s} \frac{\Theta}{\tau s + 1} \end{aligned} \quad \text{(A12)}$$

in which capital letters denote transforms of the corresponding lowercase functions and s is the transform variable. Now, since the $h_i(t)$ are normalized tracer transmit time probability density functions, their integrals on $(0, \infty)$ are unity; that is, the relations

$$H_i(O) = \int_0^\infty h_i(t) dt = 1 \qquad i = 1, 2, 3 \quad \text{(A13)}$$

all hold. Additionally, by Zierler's theorem (1965) and the central volume principle (Zierler, 1963; Roberts et al., 1973), the relations

$$Q_D^\delta(0) = \int_0^\infty q_D^\delta(t) dt = t_D = \frac{V_D}{F_S} \quad \text{(A14)}$$

also hold. In the above, t_D is the mean transmit time of tracer through D when the flow through the sampling system is F_S and the blood volume in D is V_D. Setting $s = 0$ in Eq. A12 and using Eqs. A13 and A14, we obtain the evaluation

$$\Theta = t_D \quad \text{(A15)}$$

In view of Eq. A15, Eq. A11 becomes

$$g(t; \tau, t_0, t_D) = u(t - t_0) \frac{t_D}{\tau} \exp\left(-\frac{t - t_0}{\tau}\right)$$
$$\tau > 0,\ t_0 \geq 0,\ t_D > 0 \quad \text{(A16; 2)}$$

The Laplace transform of Eq. A16 is

$$G(s;\,\tau,\,t_0,\,t_D) = e^{-t_0 s}\,\frac{t_D}{\tau s + 1}$$

Inserting this into the Laplace transform of Eq A9 and solving for the resulting transform of $\hat{p}$ gives

$$\hat{P}(s;\,\boldsymbol{x},\,\tau,\,t_0) = \frac{\epsilon_1 F}{\epsilon_2 F_s}\,\frac{1}{s}\,e^{t_0 s}\,\frac{\tau s + 1}{t_D}\,R(s)Q^{\delta}(s;\,\boldsymbol{x}) \tag{A17}$$

which, in view of Eqs. A6 and A14, reduces to

$$\hat{P}(s;\,\boldsymbol{x},\,\tau,\,t_0) = \frac{\epsilon_1}{r_\infty/c_0}\,e^{t_0 s}\left[\tau R(s) + \frac{1}{s}\,R(s)\right]FQ^{\delta}(s;\,\boldsymbol{x})$$

On taking the inverse transform of the above, we find

$$\hat{p}(t;\,\boldsymbol{x},\,\tau,\,t_0) = \frac{\epsilon_1}{r_\infty/c_0}\left[\tau r(T) + \int_0^T r(\theta)d\theta\right] * Fq^{\delta}(T;\,\boldsymbol{x})\Big|_{T=t+t_0} \tag{A18}$$

for our simulated PET response. Note that in Eq. A18 we have circumvented the need for the numerical deconvolution implied in A9 by virtue of the form A11 we chose for $g(t)$, the differential dispersion delay function. Note also that we have supplemented the original parameter list ($\boldsymbol{x}$) by including the parameters τ and t_0 and that the indicated combination in A17 of the quantities ϵ_2, F_S, and t_D reduces to the ratio of the quantities r_∞ and c_0, each of which we determine in our sampling system calibration. We mention that our approach not only avoids the necessity of performing numerical deconvolution and numerical differentiation of noisy data sequences, but obviates determination of the dynamic characteristics of the automatic blood-sampling system as well.

The observed and simulated PET counting rate values for n scan intervals $[T_i,\,T_{i-1}]$, $i = 1, 2, \cdots, n$, are given, respectively, in terms of the functions defined in Eqs. A1 and A18, by the differences

$$\Delta p_i = p(T_i) - p(T_{i-1}) \qquad i = 1, 2, \cdots, n$$

and

$$\Delta\hat{p}_i(\boldsymbol{x},\,\tau,\,t_0) = \hat{p}(T_i;\,\boldsymbol{x},\,\tau,\,t_0) - \hat{p}(T_{i-1};\,\boldsymbol{x},\,\tau,\,t_0) \qquad i = 1, 2, \cdots, n$$

Our parameter estimation procedure consists in adjusting the parameter vector ($\boldsymbol{x}$) as well as the time constant (τ) and the time shift (t_0) in the model scan simulations $[\Delta\hat{p}_i(\boldsymbol{x},\,\tau,\,t_0)]$ to obtain the best fit to the integrated PET scan data ($\Delta\hat{p}_i$) for all n time frames ($\Delta T = T_i - T_{i-1}$) of a study. (Note that in Eq. A18, F appears explicitly as well as implicitly in $\boldsymbol{x}$.)

Our method resembles those of Meyer (1989) and of Lammertsma et al. (1989, 1990) in the sense that we also employ a parameterized exponential function of time (Eqs. A11, A16; 2) to represent the effect of dispersion. Our approach differs from theirs, however, in that our data-processing algorithm based on Eq. A18 can be used with *any* blood–tissue exchange model whatsoever for which the unit impulse residue response function is at hand. For this reason, we are able to accommodate our DP model as well as our implementation of the Kety 1C. In contrast, the formulations of Meyer and of Lammertsma et al. are relevant only for the Kety 1C model.

Acknowledgment: We thank the staffs of the Washington University Medical School cyclotron and of the Radiation Sciences Division of the School's Mallinckrodt Institute of Radiology for their invaluable technical assistance. We also thank Anna Cook who processed drafts of our manuscript through several revisions. This research was supported by NIH grant nos. HL13851, NS06833, and RR01380 and the McDonnell Center for Studies of Higher Brain Function.

REFERENCES

Alpert NM, Eriksson L, Chang JY, Bergstrom M, Litton JE, Correia JA, Bohm C, Ackerman RH, Taveras JM (1984) Strategy for the measurement of regional cerebral blood flow using short-lived tracers and emission tomography. *J Cereb Blood Flow Metab* 4:28–34

Beck JV, Arnold KJ (1977) *Parameter Estimation in Engineering and Science*. New York, Wiley

Berridge MS, Cassidy EH, Perris AH (1990) A routine automated synthesis of ^{15}O-labeled butanol for positron tomography. *J Nucl Med* 31:1727–1731

Berridge MS, Adler LP, Nelson AD, Cassidy EH, Muzic RF, Bednarczyk EM, Miraldi F (1991) Measurement of human cerebral blood flow with ^{15}O-butanol and positron emission tomography. *J Cereb Blood Flow Metab* 11:707–711

Bolwig TG, Lassen NA (1975) The diffusion permeability to water of the rat blood-brain barrier. *Acta Physiol Scand* 93: 415–422

Brooks DJ, Frackowiak RSJ, Lammertsma AA, Herold S, Leenders KL, Selwyn AP, Turton DR, Brady F, Jones T (1986) A comparison between regional cerebral blood flow measurements obtained in human subjects using ^{11}C-methylalbumin microspheres, the $C^{15}O_2$ steady-state method, and positron emission tomography. *Acta Neurol Scand* 73:415–422

Carson RE, Huang SC, Green MV (1986) Weighted integration method for local cerebral blood flow measurements with positron emission tomography. *J Cereb Blood Flow Metab* 6:245–258

Eichling JO, Raichle ME, Grubb RL, Jr, Ter-Pogossian MM (1974) Evidence of the limitations of water as a freely diffusible tracer in brain of the rhesus monkey. *Circ Res* 35: 358–364

Eklöf B, Lassen NA, Nilsson L, Norberg K, Siesjö BK, Torlöf P (1974) Regional cerebral blood flow in the rat measured by the tissue sampling technique; a critical evaluation using four indicators ^{14}C-antipyrine, ^{14}C-ethanol, ^{3}H-water and ^{133}Xenon 133. *Acta Physiol Scand* 91:1–10

Fox PT, Perlmutter J, Raichle ME (1985) A stereotactic method

of anatomical localization for positron emission tomography. *J Comput Assist Tomogr* 9:141–153

Fox PT, Miezen FM, Allman JM, Van Essen DC, Raichle ME (1987) Retinotopic organization of human visual cortex mapped with positron emission tomography. *J Neurosci* 7: 913–922

Frackowiak RSJ, Lenzi GL, Jones T, Heather JD (1980) Quantitative measurement of regional cerebral blood flow and oxygen metabolism in man using ^{15}O and positron emission tomography: theory, procedure, and normal values. *J Comput Assist Tomogr* 4:727–736

Gambhir SS, Huang SC, Hawkins RA, Phelps ME (1987) A study of the single compartment tracer kinetic model for the measurement of local cerebral blood flow using ^{15}O-water and positron emission tomography. *J Cereb Blood Flow Metab* 7:13–20

Ginsberg MD, Lockwood AH, Busto R, Finn RD, Butler CM, Cendan IE, Goddard J (1982) A simplified in vivo autoradiographic strategy for the determination of regional cerebral blood flow by positron emission tomography: theoretical considerations and validation studies in the rat. *J Cereb Blood Flow Metab* 2:89–98

Ginsberg MD, Howard BE, Hassel WR (1984) Emission tomographic measurement of local cerebral blood flow in humans by an in vivo autoradiographic strategy. *Ann Neurol* 15:S12–S18

Gjedde A, Hansen AJ, Siemkowicz E (1980) Rapid simultaneous determination of regional blood flow and blood-brain glucose transfer in the brain of rat. *Acta Physiol Scand* 108: 321–330

Go KG, Lammertsma AA, Panns AMJ, Vaalburg W, Woldring MG (1981) Extraction of water labeled with oxygen 15 during single-capillary transit. *Arch Neurol* 38:581–584

Herscovitch P, Raichle ME (1983) Effect of tissue heterogeneity on the measurement of cerebral blood flow with the equilibrium $C^{15}O_2$ inhalation technique. *J Cereb Blood Flow Metab* 3:407–415

Herscovitch P, Raichle ME (1985) What is the correct value for the brain–blood partition coefficient for water? *J Cereb Blood Flow Metab* 5:65–69

Herscovitch P, Markham J, Raichle ME (1983) Brain blood flow measured with intravenous $H_2^{15}O$. I. Theory and error analysis. *J Nucl Med* 24:782–789

Herscovitch P, Raichle ME, Kilbourn MR, Welch MJ (1987) Positron emission tomographic measurement of cerebral blood flow and permeability–surface area product of water using [^{15}O]water and [^{11}C]butanol. *J Cereb Blood Flow Metab* 7:527–542

Huang S-C, Carson RE, Phelps ME (1982) Measurement of local blood flow and distribution volume with short-lived isotopes: a general input technique. *J Cereb Blood Flow Metab* 2:99–108

Huang S-C, Carson RE, Hoffman EJ, Carson J, MacDonald N, Barrio JR, Phelps ME (1983) Quantitative measurement of local cerebral blood flow in humans by positron emission computed tomography and ^{15}O-water. *J Cereb Blood Flow Metab* 3:141–153

Hutchins GD, Hichwa RD, Koeppe RA (1986) A continuous flow input function detector for $H_2^{15}O$ blood flow studies in positron emission tomography. *IEEE Trans Nucl Sci* 33:546–549

Iida H, Kanno I, Mirua S, Murakami M, Takahashi K, Uemura K (1986) Error analysis of a quantitative cerebral blood flow measurement using $H_2^{15}O$ autoradiography and positron emission tomography, with respect to the dispersion of the input function. *J Cereb Blood Flow Metab* 6:536–545

Iida H, Higano S, Tomura N, Shishido F, Kanno I, Miura S, Murakomi M, Takahashi K, Sasaki H, Uemura K (1988) Evaluation of regional differences of tracer appearance time in cerebral tissues using [^{15}O]water and dynamic positron emission tomography. *J Cereb Blood Flow Metab* 8:285–288

Iida H, Kanno I, Miura S, Murakami M, Takahashi K, Uemura K (1989) A determination of the regional brain/blood partition coefficient of water using dynamic positron emission tomography. *J Cereb Blood Flow Metab* 9:874–885

Kanno I, Lammertsma AA, Heather JD, Gibbs JM, Rhodes CG, Clark JC, Jones T (1984) Measurement of cerebral blood flow using bolus inhalation of $C^{15}O_2$ and positron emission tomography: description of the method and its comparison with $C^{15}O_2$ continuous inhalation method. *J Cereb Blood Flow Metab* 4:224–234

Kanno I, Iida H, Miura S, Murakami M, Takahashi K, Sasaki H, Inugami A, Shishido F, Uemura K (1987) A system for cerebral blood flow measurement using an $H_2^{15}O$ autoradiographic method and positron emission tomography. *J Cereb Blood Flow Metab* 7:143–153

Kety SS (1951) The theory and applications of exchange of inert gas at the lungs and tissues. *Pharmacol Rev* 3:1–41

Kety SS (1960) Measurement of local blood flow by the exchange of an inert, diffusible substance. *Methods Med Res* 8:228–236

Koeppe RA, Holden JE, Ip WR (1985) Performance comparison of parameter estimation techniques for the quantitation of local cerebral blood flow by dynamic positron computed tomography. *J Cereb Blood Flow Metab* 5:224–234

Koeppe RA, Hutchins GD, Rothley JM, Hichwa RD (1987) Examination of assumptions for local cerebral blood flow studies in PET. *J Nucl Med* 28:1695–1703

Lammertsma AA, Frackowiak RSJ, Hoffman JM, Huang S-C, Weinberg IN, Dahlbom M, MacDonald NS, Hoffman EJ, Mazziota JC, Heather JD, Forse GR, Phelps ME, Jones T (1989) The $C^{15}O_2$ build-up technique to measure regional cerebral blood flow and volume of distribution of water. *J Cereb Blood Flow Metab* 9:461–470

Lammertsma AA, Cunningham VJ, Deiber MP, Heather JD, Bloomfield PM, Nutt J, Frackowiak RSJ, Jones T (1990) Combination of dynamic and integral methods for generating reproducible functional CBF images. *J Cereb Blood Flow Metab* 10:675–686

Larson KB, Markham J, Raichle ME (1987) Tracer-kinetic models for measuring cerebral blood flow using externally detected radiotracers. *J Cereb Blood Flow Metab* 7:443–463

Marquardt DW (1963) An algorithm for least-squares estimation of nonlinear parameters. *J Soc Indust Appl Math* 11:431–441

Meyer E (1989) Simultaneous correction for tracer arrival, delay and dispersion in CBF measurements by the $H_2^{15}O$ autoradiographic method and dynamic PET. *J Nucl Med* 30:1069–1078

Petersen SE, Fox PT, Posner MI, Mintun MA, Raichle ME (1988) Positron emission tomographic studies of the cortical anatomy of single word processing. *Nature* 331:585–589

Quarles RP, Mintun MA, Larson KB, Raichle ME, Markham J (1989) Distributed and one-compartment models for estimating CBF with ^{15}O-water and PET during rest and activated states. *J Cereb Blood Flow Metab* 9(Suppl 1):S583

Raichle ME, Eichling JO, Straatmann MG, Welch MJ, Larson KB, Ter-Pogossian MM (1976) Blood-brain barrier permeability of ^{11}C-labeled alcohols and ^{15}O-labeled water. *Am J Physiol* 230:543–552

Raichle ME, Markham J, Larson K, Grubb RL Jr, Welch MJ (1981) Measurement of local cerebral blood flow in man with positron emission tomography. *J Cereb Blood Flow Metab* 1(suppl 1):S19–S20

Raichle ME, Martin WRW, Herscovitch P, Mintun MA, Markham J (1983) Brain blood flow measured with intravenous $H_2^{15}O$. II. Implementation and validation. *J Nucl Med* 24:790–798

Roberts GW, Larson KB, Spaeth EE (1973) The interpretation of mean transit time measurements for multiphase tissue system. *J Theor Biol* 39:447–475

Rose CP, Goresky CA, Bach GG (1977) The capillary and sarcolemmal barriers in the heart. An exploration of labeled water permeability. *Circ Res* 41:515–533

Schmidt K, Sokoloff L, Kety SS (1989) Effects of tissue heterogeneity on estimates of regional cerebral blood flow. *J Cereb Blood Flow Metab* 9(suppl 1):242

Shipley RA, Clark RE (1972) *Tracer Methods for In Vivo Kinetics*. New York, Academic Press

Ter-Pogossian MM, Ficke DC, Hood JT Sr, Yamamoto M, Mullani NA (1982) PETT VI: a positron emission tomograph utilizing cesium fluoride scintillation detectors. *J Comput Assist Tomogr* 6:125–133

Van Vitert RL, Levy DE (1978) Regional brain blood flow in the conscious gerbil. *Stroke* 9:67–72

Welch MJ, Kilbourn MR (1985) A remote system for the routine production of oxygen-15 radiopharmaceuticals. *J Label Comp Radiopharm* 22:1193–1200

Wise R, Chollet F, Hadar U, Friston K, Hoffner E, Frackowiak R (1991) Distribution of cortical neural networks involved in word comprehension and word retrieval. *Brain* 114:1803–1817

Zatorre RJ, Evans AC, Meyer E, Gjedde A (1992) Lateralization of phonetic and pitch discrimination in speech processing. *Science* 256:846–950

Zierler KL (1963) Theory of use of indicators to measure blood flow and extracellular volume and calculation of transcapillary movement of tracers. *Circ Res* 12:464–471

Zierler KL (1965) Equations for measuring blood flow by external monitoring of radioisotopes. *Circ Res* 16:309–321